INTERNATIONAL JOURNAL FOR NUMERICAL METHODS IN FLUIDS
Int. J. Numer. Meth. Fluids 2006; **50**:469–489
Published online 1 September 2005 in Wiley InterScience (www.interscience.wiley.com). DOI: 10.1002/fld.1069

Modelling spray impingement using linear stability theories for droplet shattering

S. S. Yoon[1,*,†] and P. E. DesJardin[2,‡]

[1] *Mechanical Engineering Department, Korea University, Anamdong, 5-Ga, Sungbukgu, Seoul, 136-713, Korea*
[2] *Department of Mechanical & Aerospace Engineering, University at Buffalo, The State University of New York, NY 14260, U.S.A.*

SUMMARY

This paper compares several linear-theory-based models for droplet shattering employed for simulations of spray impingement on flat wall surface or a circular cylinder. Numerical simulations are conducted using a stochastic separated flow (SSF) technique that includes sub-models for droplet dynamics and impact. Results for spray impingement over a flat wall indicate that the linear theory applicable for a single droplet impact over-predicts the number of satellite (or secondary) droplets upon shattering when compared to experimental data. The causes for the observed discrepancies are discussed. Numerical simulation results for spray impingement over a circular cylinder in cross flow are obtained and discussed. Copyright © 2005 John Wiley & Sons, Ltd.

KEY WORDS: shattering; splashing; finger; satellite; droplet; impact; linear theories; secondary instability; spray; distribution

1. INTRODUCTION

Spray impingement over a solid object is of interest to the fire science community. For fire suppression applications, the dynamic behaviour and distribution of spray droplets are important parameters for determining optimal fire suppression conditions. Often the prediction of spray transport within cluttered environments is of significant interest. Usually, the operating pressure is high, allowing fire suppression sprays to achieve maximum penetration in the enclosure without concern for objects that may be inside. At this high operating pressure, the

*Correspondence to: S. S. Yoon, Mechanical Engineering Department, Korea University, Anamdong, 5-Ga, Sungbukgu, Seoul, 136-713, Korea.
†E-mail: skyoon@korea.ac.kr
‡E-mail: ped3@eng.buffalo.edu

Contract/grant sponsor: United States Department of Energy: contract/grant number: DE-AC04-94AL85000
Contract/grant sponsor: Department of Defense
Contract/grant sponsor: National Science Foundation; contract/grant number: CTS-0348110

Received 17 March 2005
Revised 14 July 2005
Accepted 18 July 2005

momentum of the injected droplets is high enough that droplets shatter upon impact. In this case, droplet characteristics (i.e. size and velocity) suddenly change, resulting in unexpected fire suppression behaviour. For this reason, the characteristics of shattered droplets must be accurately predicted in order to properly describe droplet transport near the impact region.

The impact of isolated droplets has been extensively studied. The maximum spreading radius of a droplet, its relationship with the dissipated and surface energies, the impacting criteria (distinguished from droplet sticking, rebounding, and shattering), and the number of 'fingers' formed during the shattering regime are often the focus of the single droplet impact studies [1–5]. While droplet sticking and rebounding play a small role in defining the overall spray characteristics, shattering can substantially change the distribution of droplet sizes. At sufficiently high impact velocities, the droplet first splashes (a crown shape is clearly visible in the liquid–liquid impact as shown in Figure 1; splashing also does occur in the liquid–wall impact) and then attains a pancake shape (see Figure 2(a)) and then transitions into 'fingers' (see Figure 2(b)). The formation of the satellite droplets results from the growth of an azimuthal instability mode and is sometimes referred to as a 'finger' instability. The 'finger' is formed at the end of the spreading process along the pancake edge. Note that a 'cusp' is the ligament formed due to splashing from a crown.

Previous researchers estimated the number of fingers around the rim of a crown using linear stability theory. Rieber and Frohn [8] using a Rayleigh instability type of analysis showed numerically that the most unstable wavelength is $\lambda = 4.51 d_{\text{rim}}$, where d_{rim} is the thickness of the rim which can be used to predict the number of cusps, N_{c}, for a

Figure 1. Formation of satellite droplets around the 'crown' rim [6] at low-speed impact. Circumferential length of a ring with respect to the rim diameter is $l = \pi D_{\max} = 39 d_{\text{rim}}$. Applying the Rayleigh instability ($\lambda = 4.51 d_{\text{rim}}$) yields the number of satellite droplets, $N = l/\lambda \approx 9$, which seems to be in agreement with the number of satellites in this figure. Printed with the permission of Andrew Davidhazy of Rochester Institute of Technology.

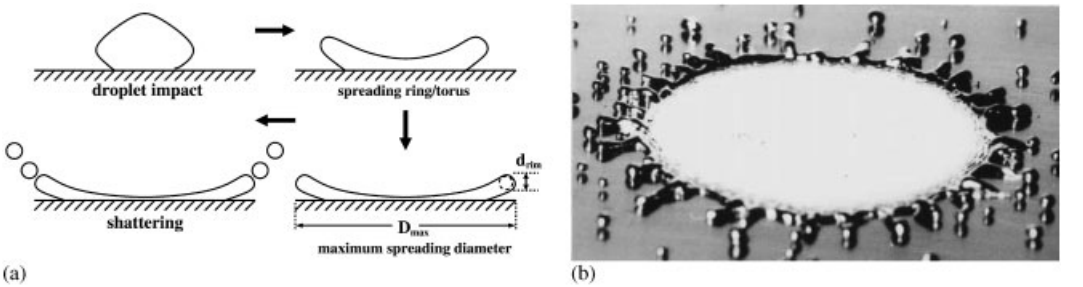

Figure 2. (a) Schematics of droplet shattering phenomenon on a solid wall; and (b) Experimental image of a shattering moltin tin droplet [7]. Reprinted by the permission of Elsevier.

water droplet impact on a water pool. Marmanis and Thoroddsen [3] showed experimentally that the number of fingers, N_f, is strongly dependent on the following parameter: $N_f \propto (0.5U/\sqrt{\nu})(\pi^2 \rho D^3/\sigma)^{0.25} \propto (We^{0.25} Re^{0.5})^{0.75}$, which includes droplet diameter (D), impact speed (U), liquid density (ρ), kinematic viscosity (ν), and surface tension (σ). Note that $N_c \neq N_f$ due to nonlinear effect during the droplet spreading (addressed in Section 2.3). Thoroddsen's subsequent work [9] reiterated the importance of viscosity, and strongly disputed Allen's theory [1] that omitted the effect of the liquid's viscosity. While the importance of viscosity was also reemphasized by Loehr and Lasek [10], Kim *et al.* [4] revisited Allen's potential flow theory and claimed that Allen's omission of viscosity was valid. Kim *et al.* [4] found that their numerical and experimental work was consistent with Allen's utilization of the Rayleigh–Taylor instability [11, 12]. Kim *et al.* [4] also found that their work was consistent with the Range and Feuillebois's experiment [13] which showed that the number of fingers was insensitive to the liquid viscosity. More recently, Mehdizadeh *et al.* [5] reconfirmed that the Rayleigh–Taylor instability is capable of accurately predicting the number of fingers for the wide range of Weber number.

In this study, the aforementioned linear theories and the empirical formula of Marmanis and Thoroddsen [3], (specifically, four different estimates of satellite droplet size) are assumed, based on: (1) the Rayleigh instability [14] used by Rieber and Frohn [8]; (2) the Rayleigh–Taylor instability of Kim *et al.* [4], Aziz and Chandra [7], and Mehdizadeh *et al.* [5]; (3) the Weber instability [15] which accounts for the liquid viscosity effect; and (4) the impact of the Reynolds number used by Marmanis and Thoroddsen [3] who emphasized the importance of liquid viscosity.

The focus of the first part of the effort is to address the pros and cons of the applied linear theories, and assess the role of viscosity in modelling droplet shattering over a solid surface with comparison to the experimental data of Powell and Lee [16]. The analysis is then extended to the case of spray impingement over a circular cylinder. Our main interest is on the effect of droplet size distributions that might be significant in fire suppression scenarios.

2. COMPUTATIONAL MODEL

2.1. Modelling background

Numerical simulations are conducted using Sandia's fire field modelling code VULCAN, which has been extended to handle the dilute multiphase flow physics found in evaporating

and reacting sprays [17]. The spray model is coupled with the Navier–Stokes solver, based on a Reynolds-averaged Navier–Stokes (RANS) formulation employing a standard k–ε turbulence closure model [18]. The gas-phase flow is calculated on a Eulerian staggered Cartesian grid using the SIMPLEC method [19].

The droplet phase evolves using a Lagrangian approach based on the stochastic separated flow (SSF) model [20, 21]. Evolution equations for collections of droplets with similar sizes and initial conditions, denoted as parcels, are used to reduce computational cost. The parcels are advanced under the influence of modelled turbulent fluctuations in the gas-phase properties. Further details may be found in Reference [16].

2.2. *Conservation of energy and mass for shattering droplet*

A droplet impact model based on the work of DesJardin and coworkers is used in this study [22]. The model is formulated using simple mass and energy conservation principles at three thermo-physical droplet states shown in Figure 3. State (1) corresponds to the pre-impact state where the droplet is assumed to be spherical in shape and its mass and energy can be expressed as follows:

$$
\begin{aligned}
m &= \rho^{(1)} V^{(1)} = \rho^{(1)} \pi D^{(1)^3}/6 \\
E &= E_{\mathrm{S}}^{(1)} + E_{\mathrm{KE}}^{(1)} = \sigma^{(1)} A^{(1)} + \rho^{(1)} V^{(1)} \left(u^{(1)^2} + v^{(1)^2} + w^{(1)^2} \right)/2 \\
&= \sigma^{(1)} \pi D^{(1)^2} + \rho^{(1)} \pi D^{(1)^3} \left(u^{(1)^2} + v^{(1)^2} + w^{(1)^2} \right)/12
\end{aligned}
\tag{1}
$$

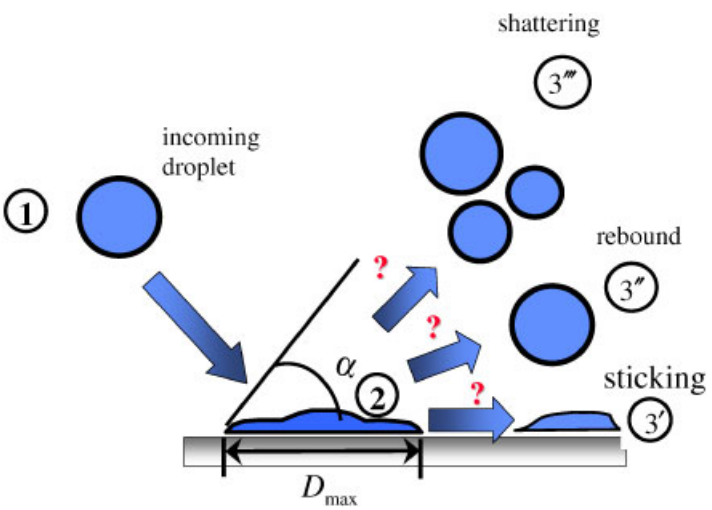

Figure 3. Configuration states during droplet impact consisting of: (1) pre-impact; (2) impact; and (3) post-impact (i.e. sticking, rebound or shattering).

where V and D are the droplet volume and diameter, respectively. E_{KE} and E_S denote the droplet kinetic and surface energies and are expressed in terms of the droplet velocity components, u, v, w, surface area, A, and liquid surface tension, σ. The superscript $(1,2,3)$ notation indicates properties of the droplet before, during and after impact, respectively. At impact state (2), the droplet is assumed to be roughly pancake shaped, with a maximum diameter equal to D_{max}. At this state, the kinetic energy of the droplet is negligible and results in only a surface energy contribution to the total energy of the droplet [23],

$$E_S^{(2)} = \frac{\pi}{4} D_{max}^2 (1 - \cos\alpha)\sigma \tag{2}$$

where α is the contact angle defined as the intersection of the tangent line at the liquid–vapour interface with the wall. The wettability (the surface roughness which affects the capability of a droplet to stick or rebound) of the cylinder increases as the droplets accumulate on the contacting surface. At steady state, droplets are essentially impacting the liquid film, rather than on a dry surface. The contact angle of $\alpha = 140^\circ$ is selected for the spray impingement on a flat surface case, based on the measurement of Aziz and Chandra [7] and Bussman *et al.* [24].

The droplet diameter at state (2) may be determined through an energy balance by equating the pre-impact energy of the droplet at state (1) to the sum of the impact energy at state (2) and the lost work due to viscous dissipation.

$$E_S^{(1)} + E_{KE}^{(1)} = E_S^{(2)} + W_{diss} \tag{3}$$

In Equation (3), W_{diss} is the work lost (or dissipated) due to viscous dissipation as the droplet undergoes deformation from states (1) to (2) and may be approximated using the relation [25],

$$W_{diss} \cong \rho\pi |U|^2 D^3 \beta_{max}^2 / (3\sqrt{Re}) \tag{4}$$

where $|U|$ is the magnitude of droplet velocity, Re is the droplet Reynolds number defined as $Re = \rho|U|D/\mu$, and β_{max} is defined as the ratio of the maximum droplet diameter at impact to its original size at state (1), i.e. $\beta_{max} = D_{max}/D$. Substituting this expression for work, along with the surface, and kinetic energy definitions of Equations (1) and (2), into Equation (4), allows for the following analytical result for β_{max} [25]:

$$\beta_{max} = \sqrt{\frac{12 + We}{3(1 - \cos\alpha) + 4\left(\frac{We}{\sqrt{Re}}\right)}} \tag{5}$$

where We is the Weber number, $We = \rho D|U|^2/\sigma$. Once β_{max} is determined, the energy at state (2) is known and will be used for determining the energy at state (3).

At state (3), one of three events is assumed to occur involving either droplet sticking, rebounding, or shattering. At very high velocities (we only consider shattering regime, excluding rebounding and sticking regimes), droplet shattering or splashing is assumed to occur if the characteristic impingement parameter, K, exceeds its critical value, $K_{crit} = 57.7$ [26], expressed in terms of the Ohnesorge number ($Oh = \sqrt{We}/Re$),

$$K = Re^{1.25} Oh = We^{0.5} Re^{0.25} \tag{6}$$

If $K > K_{crit}$, the droplet shatters (splashes). If $K < K_{crit}$, the droplet either rebounds or sticks to the surface. The critical value, $K_{crit} = 57.7$ of Mundo *et al.* [26] is applicable for a wide range of substrate roughness (for example, $10^{-3} < \gamma < 10^{0}$ where γ is the dimensionless surface roughness defined in Reference [27]) and is adopted for our current numerical simulations. However, K_{crit} increases with decreasing surface roughness substantially ($\gamma \ll 10^{-3}$) since an impacting liquid drop can spread further on a smoother surface before it shatters. Mundo *et al.* [27] noted that K_{crit} can increase up to $K_{crit} \sim 140$. Mao *et al.* [28] showed that K_{crit} can increase up to $K_{crit} \sim 152$ for a water droplet on paraffin wax surface (see Figure 7(c) of Mao *et al.* [28]).

For the case where $K > K_{crit}$ and the droplet shatters, linear theory is used to predict the number of satellite droplets, N_s, discussed further in Section 2.3. Once N_s is known, the new satellite droplet diameter is calculated using conservation of mass (i.e. $D_{sat} = D^{(1)}/N_s^{1/3}$). The surface energy of a satellite droplet is

$$E_S^{(3''')} = \pi \sigma D_{sat}^2 \tag{7}$$

The total energy at state (3‴), the sum of both surface and kinetic energies of N_s number of satellite droplets, is equal to the surface energy at state (2) accounting to energy lost through the viscous dissipation, as in Equation (4). The kinetic energy of a satellite droplet can be estimated using the principle of energy conservation:

$$E_S^{(2)} = N_s(E_{KE}^{(3''')} + E_S^{(3''')}) \tag{8}$$

Assuming that all satellite droplets have the same magnitude of kinetic energy, the magnitude of an individual satellite droplet velocity is as follows:

$$|\mathbf{u}_{sat}| = \sqrt{\frac{12E_{KE}^{(3''')}}{\pi \rho D_{sat}^{(3''')}}} \tag{9}$$

The distribution of satellite droplet velocities among its components would in general require consideration of droplet momentum conservation, requiring detailed knowledge of the forces exerted on the droplet and the break up processes over the duration of impact. This knowledge is often difficult to obtain and, may be impractical to implement for spray simulations. Alternatively, a phenomenological description is pursued. In this approach, the droplets are uniformly distributed azimuthally around the impact surface normal vector in a mean sense. This modelling is accomplished by first expressing the velocity of the satellite droplet in terms of a local surface normal coordinate system as shown in Figure 4 where the unit vectors $(\hat{e}_{||}, \hat{e}_{\perp 1}, \hat{e}_{\perp 2})$ correspond to directions along (parallel) and perpendicular to the local area vector. A random number is generated for every satellite droplet to create an azimuthally random distribution of droplets perpendicular to the surface of impact using the following relations:

$$\begin{aligned} u_{||}^{(3''')} &= |u_{sat}|\sqrt{1/3} \\ u_{\perp 1}^{(3''')} &= |u_{sat}|\sqrt{2/3}\cos(2\pi \mathrm{RN}) \\ u_{\perp 2}^{(3''')} &= |u_{sat}|\sqrt{2/3}\sin(2\pi \mathrm{RN}) \end{aligned} \tag{10}$$

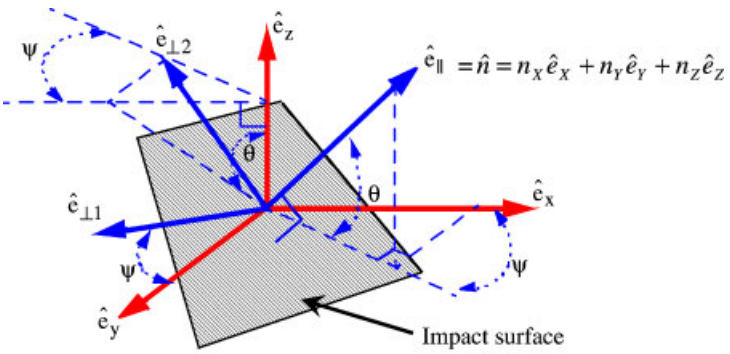

Figure 4. Relationship between impact surface and Cartesian coordinate systems.

where RN is a random number between the values of 0 and 1. The selection of the weighting factors in Equation (10) is the consequence of two conditions. The first is to ensure the kinetic energy is preserved. The second is an assumed partitioning of the kinetic energy such that 2/3 of it is from the components along the surface and 1/3 is associated with the velocity normal to the surface. The latter condition is *ad hoc* but sensitivity studies revealed that the choice of kinetic energy partitioning may not be important since the velocity of the satellite droplet is quite small and is quickly dominated by local aerodynamic drag forces. Once the velocities at state (3‴) are known from Equation (10), then velocities for the impact plane coordinate system are transformed back to a Cartesian system using the following transformation:

$$\begin{Bmatrix} u^{(3'')} \\ v^{(3'')} \\ w^{(3'')} \end{Bmatrix} = \underline{\underline{T}}^{-1} \begin{Bmatrix} u_{||}^{(3'')} \\ u_{\perp 1}^{(3'')} \\ u_{\perp 2}^{(3'')} \end{Bmatrix} = \begin{bmatrix} \cos\theta\,\cos\psi & -\sin\psi & -\sin\theta\,\cos\psi \\ \cos\theta\,\sin\psi & \cos\psi & -\sin\theta\,\sin\psi \\ \sin\theta & 0 & \cos\theta \end{bmatrix} \begin{Bmatrix} u_{||}^{(3'')} \\ u_{\perp 1}^{(3'')} \\ u_{\perp 2}^{(3'')} \end{Bmatrix} \tag{11}$$

where the directional angles θ and ψ are defined as

$$\begin{aligned} \sin\theta &= \hat{e}_{||} \cdot \hat{e}_Z \\ \cos\theta\,\sin\psi &= \hat{e}_{||} \cdot \hat{e}_Y \\ \cos\theta\,\cos\psi &= \hat{e}_{||} \cdot \hat{e}_X \end{aligned} \tag{12}$$

where $\hat{e}_{||}$ is the unit normal area vector and is known from the geometry of the impact surface.

2.3. *Prediction of satellite number using linear theories*

The most well-known droplet instability theory was developed by Rayleigh [14]. Rayleigh considered the infinitely long inviscid column of liquid with negligible influence from the gas phase, and hypothesized that an infinitesimal disturbance would cause the jet to break up under a capillary-based instability. The famous dispersion relation he obtained is

$$\omega^2 = \frac{\sigma}{\rho_l a^3}(1 - k^2a^3)\,ka\frac{I_1(ka)}{I_0(ka)} \tag{13}$$

where $\omega = \omega_r + i\omega_i$ (i.e. $\omega_r =$ growth rate, $i = \sqrt{-1}$, and $\omega_i =$ frequency of oscillation), $\sigma =$ surface tension of the liquid, $\rho_l =$ liquid density, $a = d/2$ (d is the liquid jet thickness), $k =$ wavenumber $= 2\pi/\lambda$ (i.e. $\lambda =$ wavelength), and $I_1(ka)$ and $I_0(ka)$ are modified Bessel functions of the first kind. By expanding the Bessel functions in a power series and computing the maximum of the ω vs ka curve, he obtained the result

$$\omega_{\max} = 0.97\sqrt{\frac{\sigma}{\rho_l d^3}} \tag{14}$$

for which the corresponding wavenumber and wavelength are

$$ka = 0.696 \approx 0.7 \quad \lambda = 4.51\, d \tag{15}$$

Numerous experimental confirmations of Rayleigh's wavelength exist in low-speed jets. Many researchers have extended the results to the fully nonlinear regime and have assumed that the jet will actually fragment into sections $4.51d$ in length. Rieber and Frohn [8] used the wavelength predicted by the Rayleigh theory and showed that the number of cusps (N_c) around the rim of a splashing droplet predicted by the theory was consistent with their fully 3D numerical simulation (see Table 3 in Reference [8]). A similar splashing water droplet, consistent with Rieber and Frohn's observation, is shown in Davidhazy's experiment [28] as in Figure 1. In this study we extend this idea by attempting to predict satellite droplet sizes. In this approach the geometry of the droplet after impact is envisioned as a torus shown in Figure 2(a). Certainly, not all droplets are transformed into the shape of a torus because of the change in the surface wettability and the interactions among the splashing droplets [29]. To account for the complexity induced by the evolution of the droplet impact shape, an empirical relation is needed based on the experimental observation, which is not yet available in the literature. The current assumption, therefore, provides the simplest and analytical method for modelling the satellite droplet formation.

The number of satellite droplets (N_s) is defined as the circumferential length at the maximum spreading diameter ($l = \pi D_{\max}$) divided by the most dominant wavelength (λ), i.e.

$$N_s = \pi D_{\max}/\lambda \tag{16}$$

where $D_{\max}$ is determined using Equation (5) and the diameter of the torus, d, required in Equation (17) for λ, is estimated using mass conservation resulting in $d = \sqrt{2D^3/(3\pi D_{\max})}$. It is noteworthy that the number of fingers is not equal to the number of satellite droplets (i.e. $N_f \neq N_s$), strictly speaking, due to nonlinear evolution of the liquid droplet spreading. However, as in most stability theories, linear analysis does capture the most dominant wavelength of a particular interest (see Figure 5). Thus, the nonlinear effect is assumed to be negligible for our study.

Weber [15] extended Rayleigh's analysis by adding the effect of viscosity of the jet which gives

$$\omega^2 + \frac{3\mu}{\rho_l a^2}(ka)^2\omega = \frac{\sigma}{2\rho_l a^3}(1 - k^2a^2)k^2a^2 \tag{17}$$

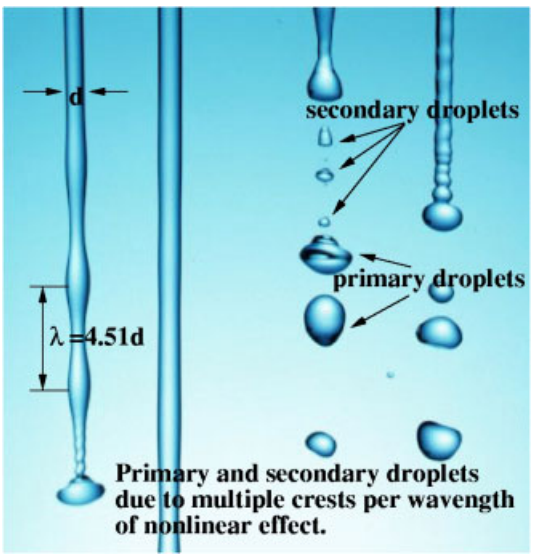

Figure 5. Typical column jet flow in the low-speed Rayleigh regime. The most dominant wavelength obeys the Rayleigh's $\lambda = 4.51d$. The secondarily small droplets are also produced due to nonlinear effect [30]. Experimental image from Reference [31]. Reprinted by permission of Begell-House.

The coefficient of the ω term accounts for viscous effects. McCarthy and Molloy [32] provided the maximum growth rate of Weber's Equation (17),

$$\omega_{\max} = \left[\sqrt{\frac{8\rho_l a^3}{\sigma}} + \frac{6\mu a}{\sigma} \right]^{-1} \tag{18}$$

The corresponding most dominant wavelength analogous to Equation (18) is

$$\frac{\lambda}{d} = \pi \sqrt{2 + \frac{6\mu}{2\rho_l a \sigma}} \tag{19}$$

and the number of droplets is determined using Equation (16), with Equation (5) used again to determine $D_{\max}$.

Allen [1] suggests that the number of satellite droplets was essentially dominated by the surface tension instability, and thus, viscosity was of little importance. He developed a criterion for the number of satellite droplets based on the Rayleigh–Taylor instability for a 2D fluid layer undergoing acceleration. Aziz and Chandra [7] later extended this analysis by assuming the acceleration of the interface, g, can be modelled as $g = U^2/D$ resulting in the following relation for the most unstable wavelength:

$$\lambda = 2\pi \sqrt{\frac{3\sigma D}{U^2 \rho}} \tag{20}$$

and found that this expression resulted in good predictions of satellite droplet numbers for various fluid types when compared to the data [7, 24].

The experimental work of Marmanis and Thoroddsen [3] and Thoroddsen and Sakakibara [9] strongly contested Allen's omission of viscosity [1]. They claimed that viscosity played an important role in droplet impact instability and provided the following relation between the impact Reynolds number and N_s, based on their experimental data:

$$N_s = 0.1 Re_I \quad Re_I = \frac{U}{2\sqrt{\nu}} \left(\frac{\pi^2 \rho D^3}{\sigma} \right)^{1/4} \tag{21}$$

More recently, Allen's Rayleigh–Taylor analysis was revisited by Kim *et al.* [4] using a radially expanding liquid jet as the baseline potential flow solution with superimposed azimuthal and radial disturbances. Analytical predictions of the number of fingers by Mehdizadeh *et al.* [5] using this theory showed that the predicted number of fingers agrees very well with their data for impacting water droplets, and they proposed the following empirical formula for the number of fingers, applicable over a wide range of Weber numbers, $10^2 < We < 5 \times 10^4$:

$$N_f = 1.14\sqrt{We} \tag{22}$$

This study assumes that the number of satellite droplets is equal to the number of fingers (i.e. $N_f = N_s$).

3. RESULTS AND DISCUSSION

3.1. Linear theory analyses

Figure 6 shows the number of satellite droplets for the linear theories discussed in Section 2.3 for a 300 μm water droplet. As is shown, the Rayleigh–Taylor wavelength predicts the largest number of satellite droplets while the predictions using Rayleigh instability theory predicts the fewest. The empirical fit to the experimental data of Mehdizadeh *et al.* [5] is essentially equivalent to the wavelength predicted by the Rayleigh–Taylor instability, and therefore, is eliminated for the sensitivity studies in Section 3.2. The Weber instability, which includes the effect of liquid viscosity, predicts the wavelength to be nearly the same as that predicted by the Rayleigh instability, and thus, the Weber equation also is eliminated for the sensitivity studies in Section 3.2. The viscosity term of the Weber wavelength in Equation (19) stabilizes the instability, therefore the wavelength is larger. For the chosen liquid (water), the viscosity plays no significant role whose fact is found when compared the wavelength of the Rayleigh equation and that of the Weber equations. Note that both the Weber and Rayleigh analyses assume that the dimensionless wavenumber, *ka*, is relatively small; therefore only large wavelengths are considered (i.e. $\lambda = 2\pi/k \gg a$). The Rayleigh–Taylor wavelength has the smallest wavelength when compared with others. The length scale of Marmanis–Thoroddsen [3] which addresses the importance of viscosity, similar to the Weber equation, is somewhat of a compromise between the large wavelengths (Rayleigh and Weber) and the small wavelengths (Rayleigh–Taylor).

3.2. Modelling spray impingement over a flat surface

To validate the applicability of the linear theories, a simple droplet impingement over a flat surface is simulated. Figure 7 is an experimental image of a spray impingement, taken

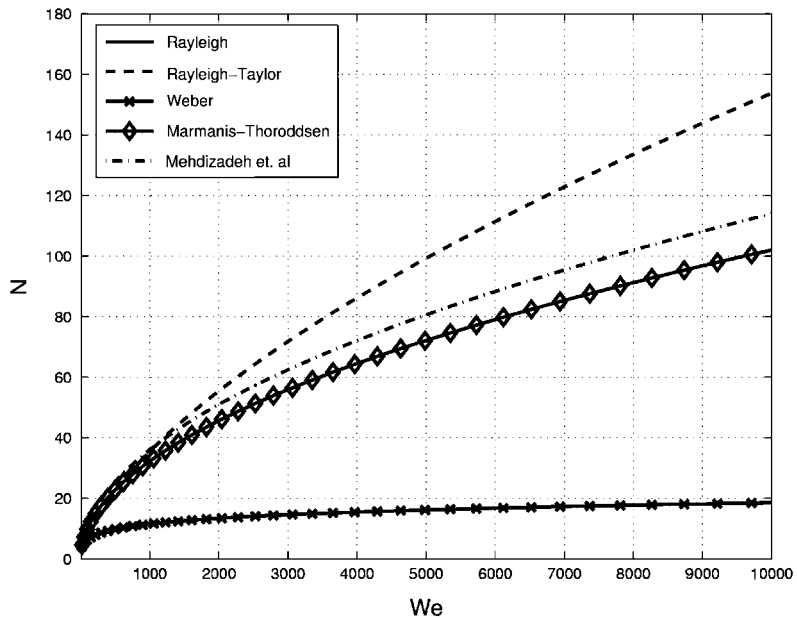

Figure 6. The prediction of satellite droplet number using various linear theories. The initial droplet size of $D = 300\,\mu\text{m}$ is used. The liquid is water. Note that the Rayleigh solution (solid line) is overlapped with that of the Weber equation.

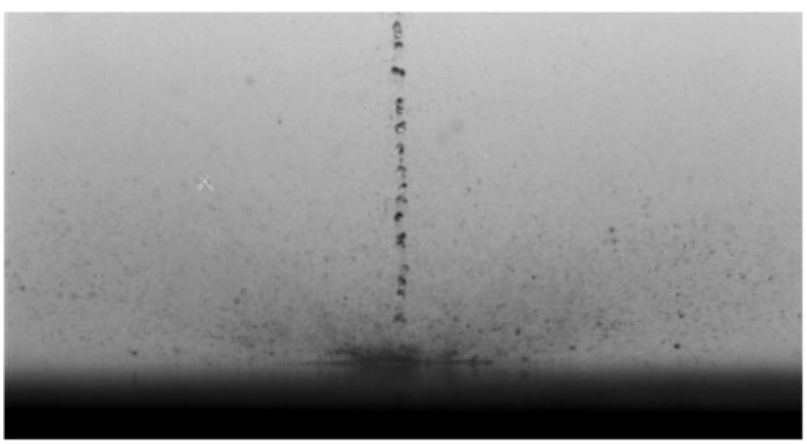

Figure 7. Experimental snapshot at 10 ms for the injected iso-octane fuel droplets over the flat Plexiglas surface [16]. Effective cone angle is 1.7°. The domain of the experimental image is $52\,\text{mm} \times 26\,\text{mm}$. Courtesy of J. Powell of University of Illinois at Urbana-Champaign.

from Reference [33]. Shattered droplets bounce off at skewed angles subsequent to impact; these shattered droplets are significantly smaller than the incoming primary droplets. Powell and Lee's data [16] indicate that the satellite droplet ranged around $0.1 \leqslant D_{\text{sat}}/D \leqslant 0.25$ for

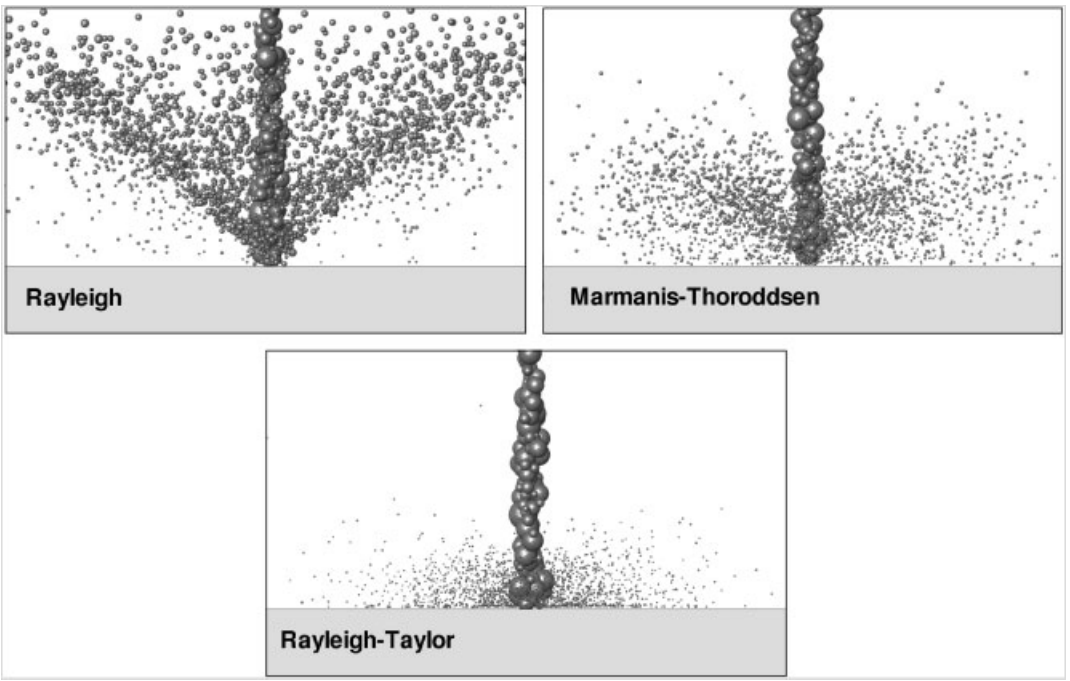

Figure 8. Modelling snapshots at 10 ms using various linear theories (Rayleigh and Rayleigh–Taylor) and the empirical formula of Marmanis–Thoroddsen [3]. The 52 mm × 26 mm 2D (x–z) views are obtained at the cross-section of $y = 0$. The liquid is iso-octane.

iso-octane droplets (whose properties are $\rho_{iso} = 692\,kg/m^3$, $\nu_{iso} = 4.6 \times 10^{-7}\,m^2/s$, and $\sigma_{iso} = 0.022\,kg/s^2$) impinging on a Plexiglas surface.

Modelling is conducted with the initial condition of the Sauter mean diameter, $D_{32} = 300\,\mu m$, taken from the experimental data obtained by Powell and Lee [16]. Using the initialization technique of Yoon *et al.* [34], the initial arithmetic mean diameter is $D_{10} = 184\,\mu m$ when using $D_{32} = 300\,\mu m$ and the Rosin–Rammler dispersion coefficient, $q = 1.77$, obtained from Reference [35]. The experimental set-ups (i.e. mass flow rate, operating pressure, injector type, etc.) of Powell and Lee [16, 33] were quite similar to those of Trujillo *et al.* [35] (private communication with J. Powell of UIUC). The mass flow rate was $\dot{m} = 0.00144\,kg/s$ with 8.45 ms injection period with 12.16 mg/injection pulsed pintle injector [16]. The computational domain for our simulation extends $0.2\,m \times 0.2\,m \times 0.1\,m$ using a $40 \times 40 \times 20$ grid, and is consistent with the computation nodes used by Trujillo *et al.* [35].

Figure 8 shows snapshots of the predicted spray impingement using the Rayleigh, Rayleigh–Taylor and Marmanis–Thoroddsen models. As expected, the Rayleigh theory over-predicts the satellite droplet size (see Figure 9) and as a result, also over-predicts their momentum. Consequently, the snapshots are not similar to the experimental image shown in Figure 7. The modelling result obtained using the Rayleigh–Taylor and Marmanis–Thoroddsen theories seems to be relatively comparable to the experimental image shown in Figure 7. The quantitative comparison shown in Figure 9 indicates that the Rayleigh–Taylor theory under-predicts

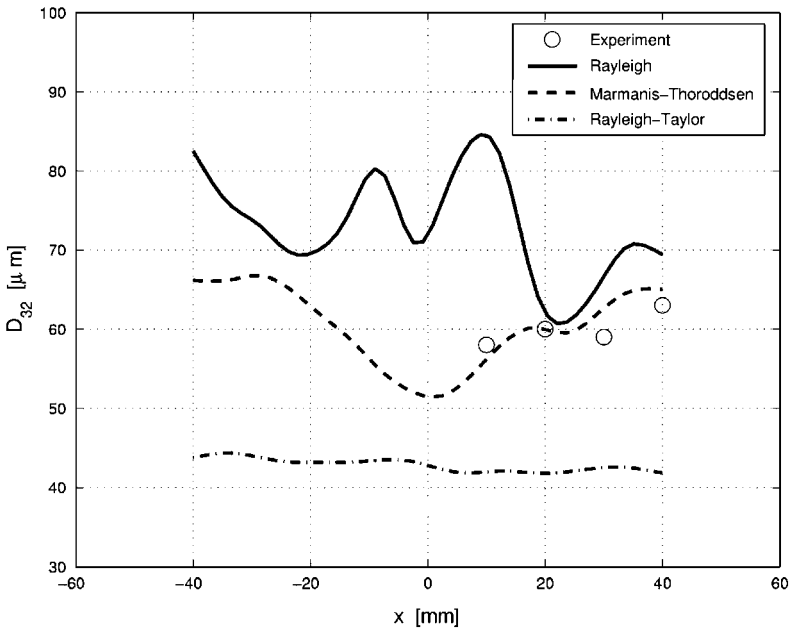

Figure 9. The comparison for the Sauter mean diameter, D_{32}, using various linear theories. Statistics are taken over the radial direction (x) at vertical height, $z = 5$ mm. The liquid is iso-octane.

the satellite droplet size when compared with the Powell and Lee's experimental data [16]. Moreover, the Sauter mean diameter (D_{32}) increases with respect to the radial direction (x) and is not captured using the Rayleigh–Taylor instability, while the experimental data indicate that larger droplets tend to travel further in the radial direction due to their higher momentum. Even though the Rayleigh–Taylor theory accurately predicts the number of satellite droplets from a single droplet impact [4, 5, 7], the theory over-estimates the satellite number (or under-predicts the satellite droplet size) for the chosen test case [16]. It should be noted that the experiments of Kim *et al.* [4], Mehdizadeh *et al.* [5], and Aziz and Chandra [7], and were carefully conducted for a single droplet impact while the case shown in Figures 7 and 8 is the spray impingement of poly-dispersed droplets continuously injected for a certain interval. It is noted that the additional experimental work on the spray impingement over a flat can be found in Reference [36].

3.3. Modelling spray impingement over a circular cylinder

3.3.1. Computation details. We extend our simulation capabilities to the case of a spray impingement over a circular cylinder for the experimental conditions of Presser *et al.* [37]. All simulations are performed for a duration of two physical seconds on a $0.48\,\text{m} \times 0.30\,\text{m} \times 0.30\,\text{m}$ ($-0.18\,\text{m} < x < 0.3\,\text{m}$, $-0.15\,\text{m} < y < 0.15\,\text{m}$, and $-0.15\,\text{m} < z < 0.15\,\text{m}$) domain to allow for initial flow transients to move out of the computational domain, and to collect data to construct time-averaged statistics. The constant free-stream air velocity, $u_\infty = 4\,\text{m/s}$, is specified at the inlet which modelled the grid-generated turbulence of the wire mesh screen (see spray injection plane in Figure 10) with the specified turbulence level of $\text{TKE} = 0.194\,\text{J/kg}$

Figure 10. View of the injected water spray over the unheated cylinder of experiment [37]. Effective cone angle is 20°.

(turbulence kinetic energy) and TDE = 0.470 J/kg (turbulent dissipation energy) to best match the experimental conditions. When adopting u_∞ as a mean streamwise velocity, the flow Reynolds number based on cylinder diameter is $Re_{\text{flow}} = u_\infty D_{\text{cyl}}/\nu_{\text{air}} = 8767$. A $70 \times 50 \times 50$ Cartesian grid is employed (thus, the total number of computational nodes is 175 000) with grid stretching employed around the cylinder to capture relevant details of the flow-to-wall boundary layer. The initial spray angle of 5° is chosen so all droplets are in collision against the frontal surface of the circular cylinder whose centre of mass is located at $x = z = 0$ in the $y = 0$ plane. Two different values of the operating mass flow rate are considered in order to investigate the growth rate amplification of the linear theories with increasing the droplet impact Weber number (i.e. $We \propto U^2$). The applied operating mass flow rate is $\dot{m} = 3.927 \times 10^{-3}$ kg/s and $\dot{m} = 7.854 \times 10^{-3}$ kg/s, which correspond to the injection liquid speed, $U_{\text{inj}} = 20$ m/s and $U_{\text{inj}} = 40$ m/s, respectively, for the given nozzle diameter, $d = 0.5$ mm. Each simulation is conducted by running an unsteady RANS simulation and collecting ensemble statistics after an initial time of $t = 0.5$ s when the flow attained a statistical stationary state. Statistics are collected from $t = 0.5$ to 2.0 s at the intervals of 0.0002 s; thus, 7500 statistic collection frequency is applied during 1.5 s. The average droplet Reynolds, and Weber number for the given operating conditions are $Re = U_{\text{inj}} D_{10}/\nu = 1594$, $Re = 3189$ and $We = \rho U_{\text{inj}}^2 D_{10}/\sigma = 487$, $We = 1947$. The corresponding Ohnesorge number for both operating conditions is $Oh = \sqrt{We}/Re \approx 0.01384$.

It is noted that the experimental image shown in Figure 10 is obtained from Reference [38]. In their case, the spray injection velocity was not high enough to result in the 'shattering' regime. The characteristic impingement parameter was $K < 57.7$ that only the droplet 'rebounding' and 'sticking' occurred in the case of Yoon *et al.* [38] while our investigation is focused on the shattering regime whose range is $0 < K < 300$ for $U_{\text{inj}} = 20$ m/s and $0 < K < 600$ for $U_{\text{inj}} = 40$ m/s.

3.3.2. Initial conditions. The spray injection is initiated at locations $x = -0.18$ m and $y = z = 0.0$ m. To represent conditions at the nozzle exit, presumed-shape droplet size and velocity distributions are often used. There are many known droplet size distribution functions such as normal, log-normal, root-normal, Rosin–Rammler, Nukiyama–Tanasawa, and

log-hyperbolic [39]. We have chosen the Rosin–Rammler distribution (whose input parameters are X and q) since the distribution was shown to have merits in modelling the initial conditions for the nozzle-type selected by Yoon *et al.* [38]. The boundary of the numerical simulation starts at the position of the nozzle exit. We have chosen the mean droplet diameter at the nozzle exit to be $X = 100\,\mu\text{m}$, one of the input parameters for the Rosin–Rammler distribution. The value of $q = 3$ is chosen based on the PDPA (phase Doppler particle analyser) measurement of Yoon *et al.* [38]. For the given dispersion coefficient, $q = 3$, the arithmetic mean diameter is $D_{10} = X\Gamma(1/q + 1) = 89.3\,\mu\text{m}$ at the nozzle exit.

3.3.3. Computational results. It is mentioned in Section 3.3.1 that the cone angle is set as $\theta = 5°$ to force all injected droplets into collision with the cylinder. When a large portion of the injected droplets deflects around the cylinder without collision at large cone angles, these deflected droplets are mixed with the shattered droplets behind the cylinder, and thus, the sole effect of the shattered droplets is difficult to observe (see Figure 11).

Figure 12 shows the variation of the Sauter mean diameter, D_{32}, over the axial domain at the vertical location of $z = 40\,\text{mm}$ for two different injection conditions, (a) $U_{\text{inj}} = 20\,\text{m/s}$ and (b) $U_{\text{inj}} = 40\,\text{m/s}$. For the quantitative comparisons, the vertical location of $z = 40\,\text{mm}$ is selected because the frequency of the droplet presence is maximized at that location.

The computational results are obtained using the Rayleigh, Marmanis–Thoroddsen, and Rayleigh–Taylor theories. The Weber equation is not considered in this case because its solution is essentially identical to that of the Rayleigh theory for the chosen liquid (water). Viscosity does not play an important role in the flow regime considered in this section, especially for theories concerned with larger wavelengths such as the Rayleigh and Weber instability theories (i.e. $ka \to 0$).

As expected, the Sauter mean diameter decreases in the choice order of the Rayleigh, Marmanis–Thoroddsen, and Rayleigh–Taylor theories. The differences between the Marmanis–Thoroddsen and Rayleigh–Taylor theories increase with increasing injection speed (compare Figures 12(a) and (b)). The 'U'-shaped profile of D_{32} in Figure 12 is attributed to the effect

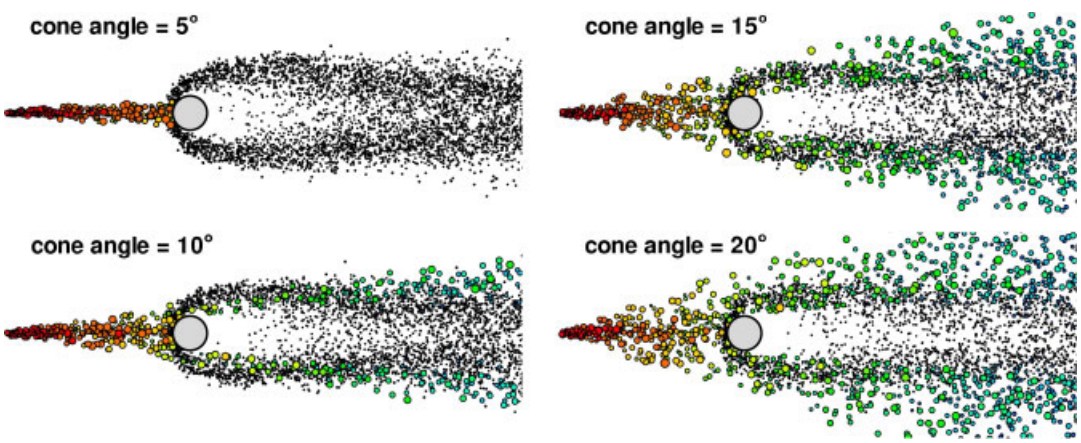

Figure 11. Different droplet characteristics behind cylinder using various injecting cone angles for the shattering droplets.

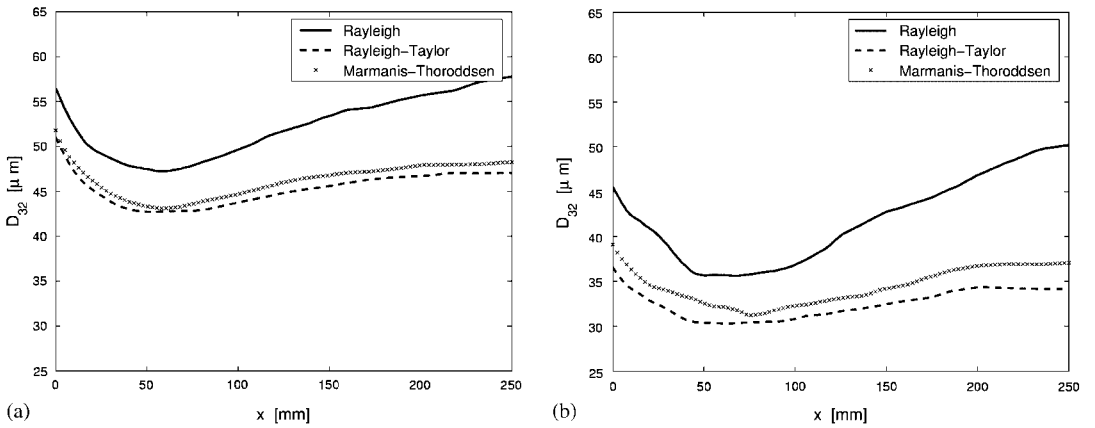

Figure 12. The variation of the Sauter mean diameter, D_{32}, over the axial direction (x) at the vertical location of $z = 40$ mm: (a) The injection speed is $U_{\text{inj}} = 20$ m/s; and (b) the injection speed is $U_{\text{inj}} = 40$ m/s.

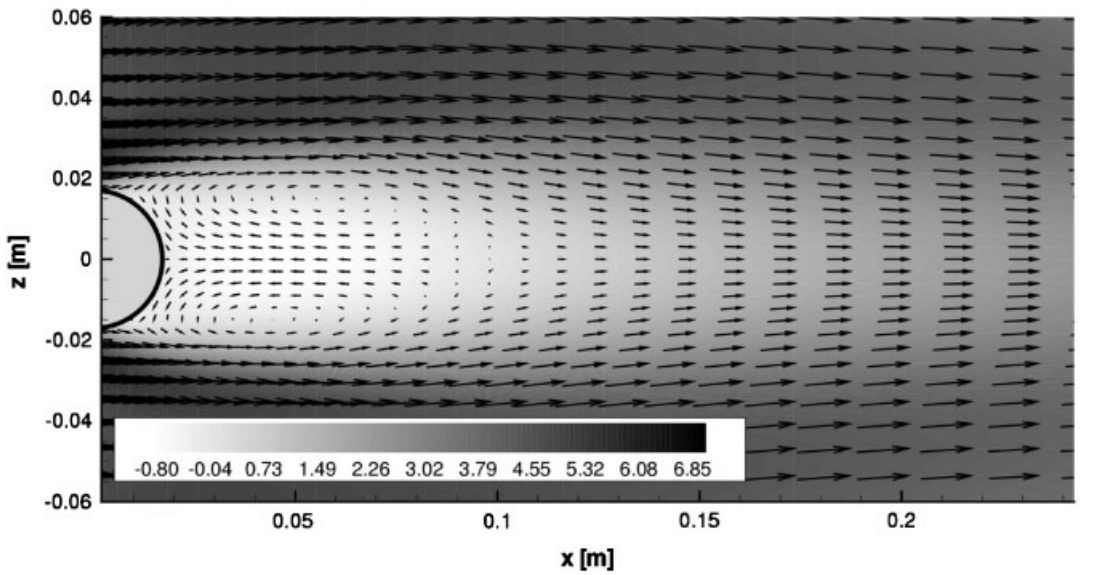

Figure 13. Velocity vector around the cylinder: recirculation zone is developed behind the cylinder. The contour colour is scaled with the flow axial velocity in the unit of (m/s). The injection speed is $U_{\text{inj}} = 20$ m/s. The empirical formula of Marmanis–Thoroddsen is used.

of the recirculation zone behind the cylinder shown in Figure 13 which serves to trap smaller droplets behind the cylinder.

The axial velocity profiles of the shattered droplets are shown in Figures 14(a) and (b) for two different injection conditions, $U_{\text{inj}} = 20$ and 40 m/s. The increase in U around the cylinder

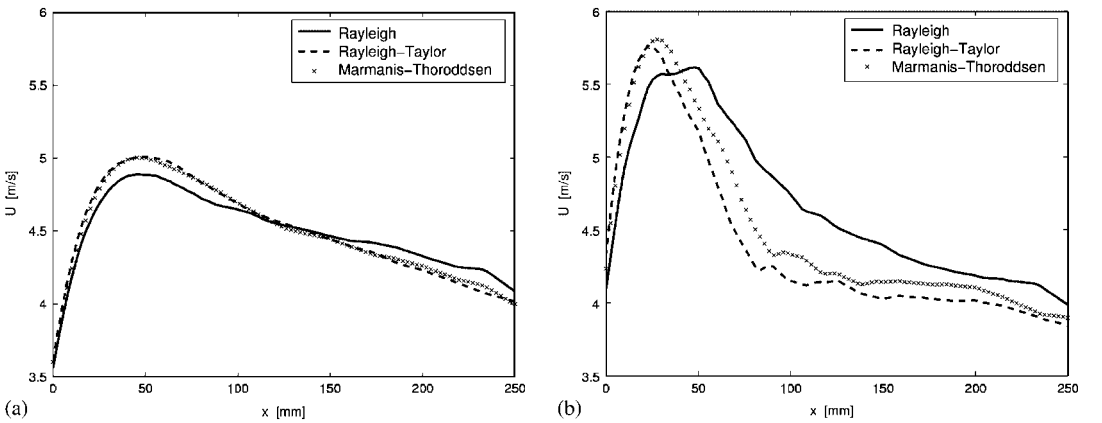

Figure 14. The variation of the droplet axial velocity, U, over the axial direction (x) at the vertical location of $z = 40\,\text{mm}$: (a) The injection speed is $U_{\text{inj}} = 20\,\text{m/s}$; and (b) the injection speed is $U_{\text{inj}} = 40\,\text{m/s}$.

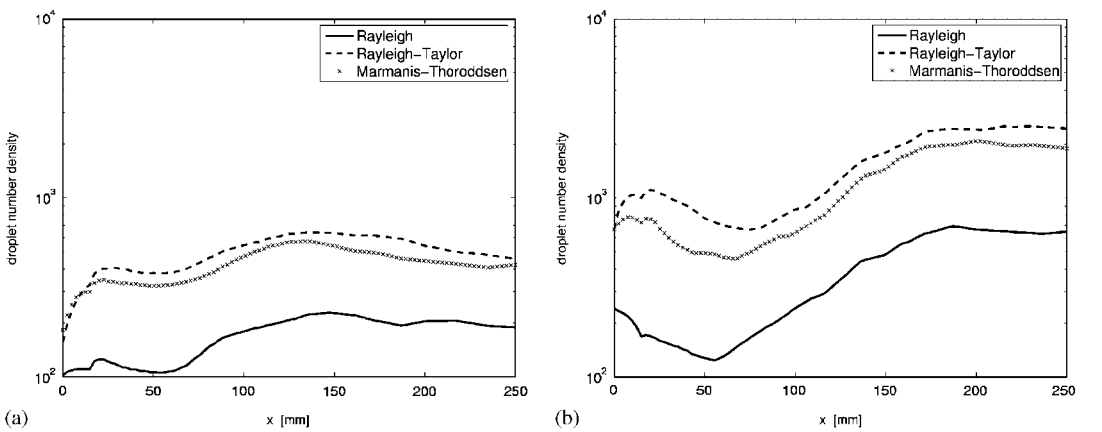

Figure 15. The variation of the droplet number density over the axial direction (x) at the vertical location of $z = 40\,\text{mm}$: (a) The injection speed is $U_{\text{inj}} = 20\,\text{m/s}$; and (b) the injection speed is $U_{\text{inj}} = 40\,\text{m/s}$.

results in an acceleration of the shattered droplets. As the axial location increases, the droplet velocity is reduced due to drag and finally reaches the free-stream velocity of $u_\infty = 4\,\text{m/s}$ in the downstream location. The resulting differences among the applied theories are prominent in Figure 14(b), while the differences are quite small in the case of Figure 14(a). The droplet distribution of the Rayleigh–Taylor theory is more sensitive to the flow environment due to the droplets' light masses, so, their decrease in velocity is more rapid compared to results using other theories since the rate of velocity reduction is proportional to the inverse of droplet size.

The droplet number density is plotted for various theories in Figure 15. As expected, the droplet number density is greatest for the Rayleigh–Taylor theory because it produces the

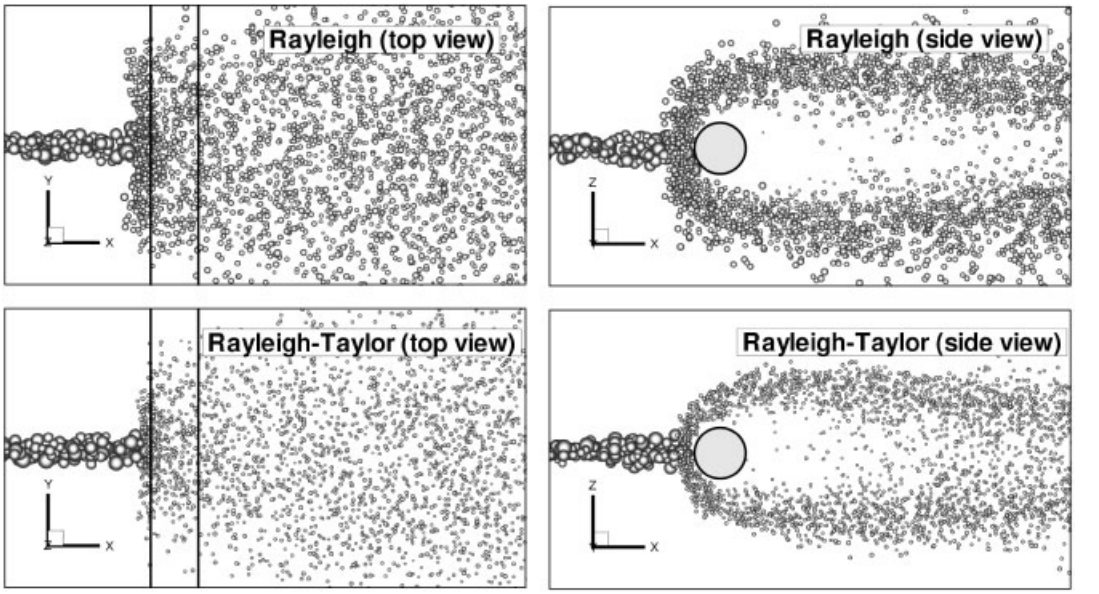

Figure 16. 3D snapshots of the droplet distribution comparison between Rayleigh and Rayleigh–Taylor linear theories. The satellite droplet size using the Rayleigh theory is over-predicted as compared to that predicted when using the Rayleigh–Taylor theory.

smallest droplet for the given mass flow rate. The snapshot of the comparison between the Rayleigh and the Rayleigh–Taylor theories is plotted in Figure 16, which shows a significant difference in droplet characteristics behind the cylinder.

The joint probability density functions (JPDF) of the satellite droplets are shown for various theories in Figure 17. All three theories indicate that the larger droplets tend to have a greater velocity following the impact. A more uniform JPDF (lesser number of size spectrum) is shown as the overall droplet size is reduced (i.e. Rayleigh $\rightarrow$ Marmanis–Thoroddsen $\rightarrow$ Rayleigh–Taylor).

4. CONCLUSIONS

Several linear theories have been implemented and tested for simulating shattering of droplets from a turbulent water spray over both a flat surface and a circular cylinder. A stochastic separated flow (SSF) technique that includes sub-models for droplet dynamics is applied for the simulation. The new droplet-shattering model is developed for the simulation of the poly-dispersed spray. Comparison between the numerical results and the experimental data indicate that the empirical formula of Marmanis and Thoroddsen [3] gives the best prediction for the satellite droplet numbers and their subsequent transport. Though the viscosity effect can be neglected for relatively low viscous liquids (such as water or gasoline), viscosity tends to dampen the instability and reduce the satellite number for highly viscous liquids. That viscosity reduces satellite numbers is also manifested in the comparison between the Rayleigh and Weber

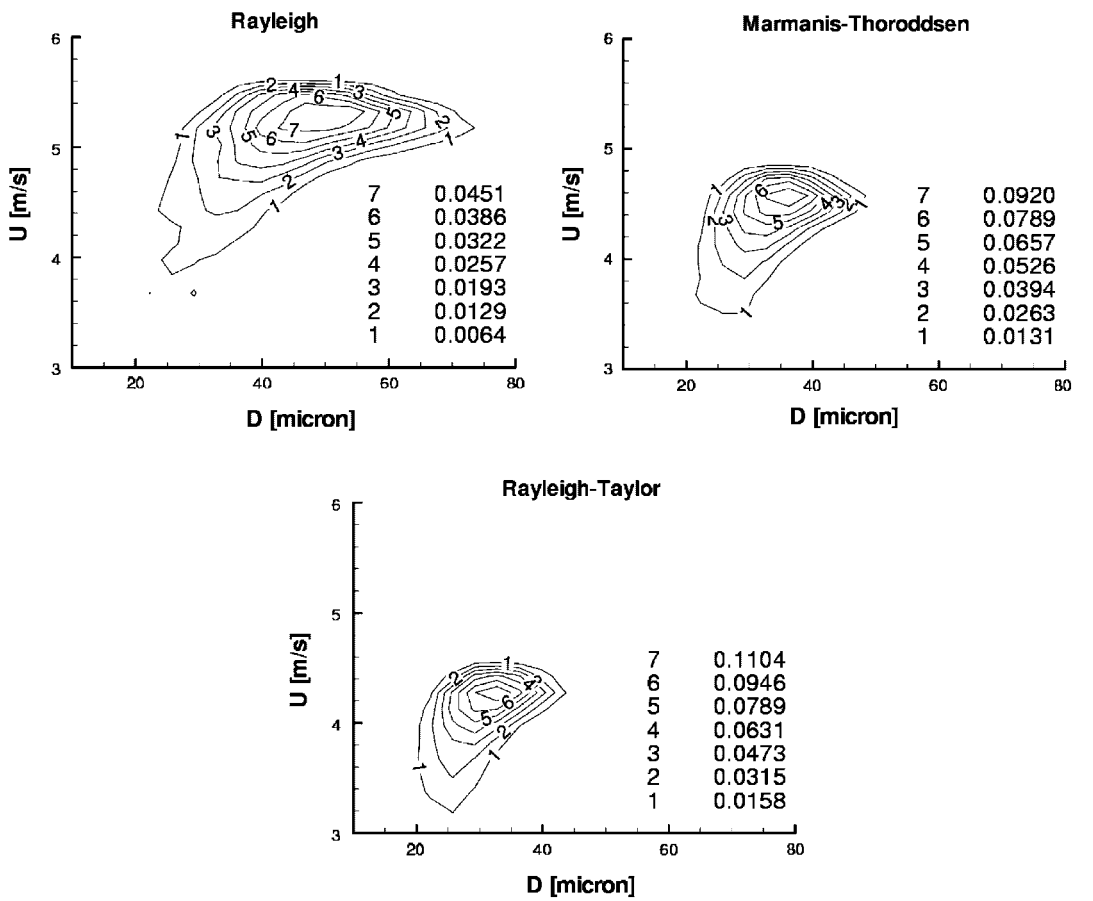

Figure 17. Joint PDFs of satellite droplet size and velocity for various linear theories.

equations. For the poly-dispersed spray impingement involving thousands of droplets, the empirical relation from Reference [3] gave the best prediction when compared with the experimental data of Powell and Lee [16]. Numerical simulation is extended for the spray impingement over a circular cylinder case for the purpose of fire suppression application. The numerical results are obtained for the potential quantitative comparison with the experimental data.

NOMENCLATURE

- a a half of liquid ring/rim thickness, $a = d/2$
- d liquid ring/rim thickness
- D droplet diameter
- k wavenumber
- K characteristic impingement parameter
- l circumferential length of a ring/torus defined as $l = \pi D_{\max}$

$N_{c,f,s}$ number of cusp, finger, and satellite droplets
Oh Ohnesorge number defined as $Oh = \sqrt{We}/Re$
Re Reynolds number defined as $Re = \rho UD/\mu = UD/\nu$
U droplet velocity
We Weber number defined as $We = \rho U^2 D/\sigma$

Greek letters

γ dimensionless surface roughness
λ wavelength
μ dynamic viscosity
ν kinematic viscosity defined as $\nu = \mu/\rho$
ω growth rate
ρ liquid density
σ surface tension

Subscripts

$()_g$ gas property
$()_l$ liquid property
$()_{max}$ maximum spreading condition of a droplet upon impact
$()_{rim}$ ring (or 'crown' rim) property
$()_{sat}$ satellite (or 'finger') droplet property

ACKNOWLEDGEMENTS

The first author acknowledges that this research was conducted during his stay at Sandia National Laboratories. Sandia is a multiprogram laboratory operated by Sandia Corporation, a Lockheed Martin Company for the United States Department of Energy's National Nuclear Security Administration under contract DE-AC04-94AL85000. The authors wish to acknowledge the partial support of this research by the Department of Defense Next Generation Fire Suppression Technology Program, funded by the DoD Strategic Environmental Research and Development Program. The second author acknowledges the support of National Science Foundation under Grant No. CTS-0348110. The authors also are grateful to the experimental information provided by Mr J. Powell of University of Illinois at Urbana-Champaign.

REFERENCES

1. Allen RF. The role of surface tension in splashing. *Journal of Colloid and Interface Science* 1975; **51**: 2350–2351.
2. Chandra S, Avedisian CT. On the collision of a droplet with a solid surface. *Proceedings of the Royal Society of London, Series A* 1991; **432**:12–41.
3. Marmanis H, Thoroddsen ST. Scaling of the fingering pattern of an impacting drop. *Physics of Fluids* 1996; **8**:1344–1346.
4. Kim HY, Feng ZC, Chun JH. Instability of a liquid jet emerging from a droplet upon collision with a solid surface. *Physics of Fluids* 2000; **12**:531–541.
5. Mehdizadeh NZ, Chandra S, Mostaghimi J. Formation of fingers around the edges of a drop hitting a metal plate with high velocity. *Journal of Fluid Mechanics* 2004; **510**:353–373.
6. Davidhazy A. 1996. http://www.rit.edu/~andpph/
7. Aziz SD, Chandra S. Impact, recoil and splashing of molten metal droplets. *International Journal of Heat and Mass Transfer* 2000; **43**:2841–2857.

8. Rieber M, Frohn A. A numerical study on the mechanism of splashing. *International Journal of Heat and Fluid Flow* 1999; **20**:455–461.
9. Thoroddsen ST, Sakakibara J. Evolution of the fingering pattern of an impacting drop. *Physics of Fluids* 1998; **10**:1359–1374.
10. Loehr KF, Lasek A. Splashing of drops. *Archives of Mechanics* 1990; **42**:507–513.
11. Aref H, Tryggvason G. Vortex dynamics of passive and active interfaces. *Physica D* 1984; **12**:59–70.
12. Sharp DH. An overview of Rayleigh–Taylor instability. *Physica D* 1984; **12**:3–18.
13. Range K, Feuillebois F. Influence of surface roughness on liquid drop impact. *Journal of Colloid and Interface Science* 1998; **203**:16–30.
14. McCarthy MJ, Molloy NA. Review of stability of liquid jets and the influence of nozzle design. *Chemical Engineering Journal* 1974; **7**:1–20.
15. Weber C. Zum zerfall eines flussigkeitsstrahles. *Zeitschrift fur Angewandte Mathematik und Mechanik* 1931; **11**:138–245.
16. Powell J, Lee CF. Impingement of a polydisperse pulsed spray on a dry wall. *15th Annual Conference on Liquid Atomization and Spray Systems*, Madison, WI, May 2002.
17. DesJardin PE, Gritzo LA. A dilute spray model for fire simulations: formulation, usage and benchmark problems. *Technical Report No. SAND2002-3419*, Sandia National Laboratories, Albuquerque, NM, 2002.
18. Jones WP, Launder BE. The prediction of laminarization with a two-equation model of turbulence. *International Journal of Heat and Mass Transfer* 1972; **15**:301–314.
19. Patankar SV. *Numerical Heat Transfer and Fluid Flow*. Taylor & Francis: New York, 1980.
20. Faeth GM. Evaporation and combustion in sprays. *Progress in Energy and Combustion Science* 1983; **9**:1–76.
21. Faeth GM. Mixing, transport and combustion in sprays. *Progress in Energy and Combustion Science* 1987; **13**:293–345.
22. DesJardin PE, Presser C, Disimile, PJ, Tucker JR. A phenomenological droplet impact model for Lagrangian spray transport. *AIAA Paper 2003-1322*, *41st AIAA Aerospace Sciences Meeting and Exhibit*, 2003.
23. Ford RE, Furmidge CGL. Impact and spreading of spray drops on foliar surfaces. In *Monograph*, Wetting SCI (ed.), vol. 25. Society of Chemical Industry, 1967; 417–432.
24. Bussman M, Chandra S, Mostaghimi J. Modelling the splash of a droplet impacting a solid surface. *Physics of Fluids* 2000; **12**:3121–3132.
25. Pasandideh-Fard M, Qiao YM, Chandra S, Mostaghimi J. Capillary effects during droplet impact on a solid surface. *Physics of Fluids* 1996; **8**:650–659.
26. Mundo C, Sommerfeld M, Tropea C. Droplet-wall collisions: experimental studies of the deformation and breakup process. *International Journal of Multiphase Flow* 1995; **21**(2):151–173.
27. Mundo C, Sommerfeld M, Tropea C. On the modelling of liquid sprays impinging on surfaces. *Atomization and Sprays* 1998; **8**:625–652.
28. Mao T, Kuhn D, Tran H. Spread and rebound of liquid droplets upon impact on flat surfaces. *AIChE Journal* 1997; **43**(9):2169–2179.
29. Sivakumar D, Tropea C. Splashing impact of a spray onto a liquid film. *Physics of Fluids* 2002; **14**(12): L85–L88.
30. Lafrance P. Nonlinear breakup of a laminar liquid jet. *Physics of Fluids* 1975; **18**:428–432.
31. Yoon SS, Heister SD. Categorizing linear theories for atomizing round jets. *Atomization and Sprays* 2003; **13**:499–516.
32. McCarthy MJ, Molloy NA. Review of stability of liquid jets and the influence of nozzle design. *Chemical Engineering Journal* 1974; **7**:1–20.
33. Powell J, Lee CF. Experimental top and side view pictures of an impinging fuel spray. *15th Annual Conference on Liquid Atomization and Spray Systems*, Madison, WI, May 2002.
34. Yoon SS, Hewson JC, DesJardin PE, Glaze DJ, Black AR, Skaggs RR. Numerical modelling and experimental measurements of a high speed solid-cone water spray for use in fire suppression applications. *International Journal of Multiphase Flow* 2004; **30**:1369–1388.
35. Trujillo MF, Mathews WS, Lee CF, Peters JE. Modelling and experiment of impingement and atomization of a liquid spray on a wall. *International Journal of Engine Research* 2000; **1**(1):87–105.
36. Panao MRO, Moreira ALN. Experimental study of the flow regimes resulting from the impact of an intermittent gasoline spray. *Experiments in Fluids* 2004; **37**:834–855.
37. Presser C, Widmann JF, DesJardin PE, Gritzo LA. Measurements and numerical predictions of liquid agent dispersal around solid obstacles. *Proceedings of the 11th Halon Options Technical Working Conference* (*HOTWC-2001*). New Mexico Engineering Research Institute: Albuquerque, NM, 2001; 122–130.
38. Yoon SS, DesJardin PE, Hewson JC, Presser C, Avedisian T. Numerical modelling and experimental measurements of water spray impact and transport over a cylinder. *International Journal of Multiphase Flow*, accepted.
39. Babinsky E, Sojka PE. Modelling drop size distributions. *Progress in Energy and Combustion Science* 2002; **28**:303–329.

